Nanoscale

Accepted Manuscript

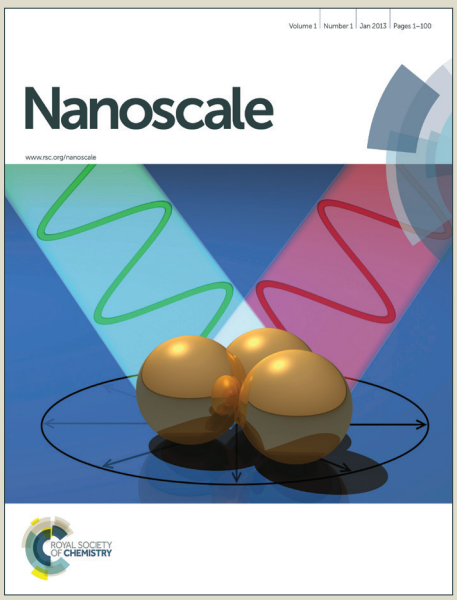

ROYAL SOCIETY OF CHEMISTRY

www.rsc.org/nanoscale

IR excitation

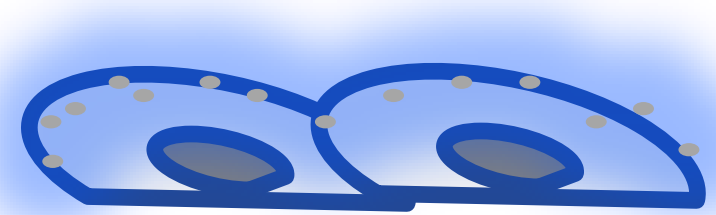

→ Imaging

Visible excitation

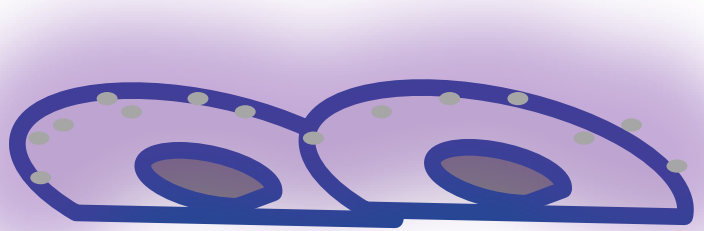

→ Direct DNA photo-interaction

Deep UV Generation and Direct DNA Photo-Interaction by Harmonic Nanoparticles in Labelled Samples

Davide Staedler,[a]‡ Thibaud Magouroux[b]‡ Solène Passemard,[a] Sebastian Schwung,[c] Marc Dubled,[d] Guillaume Stéphane Schneiter,[a] Daniel Rytz,[c] Sandrine Gerber-Lemaire,[a] Luigi Bonacina,*[b] and Jean-Pierre Wolf[b]

Received Xth XXXXXXXXXX 20XX, Accepted Xth XXXXXXXXX 20XX
First published on the web Xth XXXXXXXXXX 200X
DOI: 10.1039/b000000x

A biophotonics approach based on the nonlinear optical process of second harmonic generation is presented and demonstrated on malignant human cell lines labelled by harmonic nanoparticles. The method enables independent imaging and therapeutic action, selecting each modality by simply tuning the excitation laser wavelength from infrared to visible. In particular, the generation of deep ultraviolet radiation at 266 nm allows directly interacting with nuclear DNA in absence of photosensitizing molecules.

1 Introduction

We demonstrate here a diagnostic and therapeutic protocol based on the nonlinear optical process of non phase-matched second harmonic (SH) generation by non-centrosymmetric nanoparticles, referred to in the following as harmonic nanoparticles (HNPs).[1,2] To date, the capability of these recently introduced nanometric probes of doubling *any* incoming frequency has not been employed for therapeutic use, although it presents several straightforward advantages, including i) the possibility to directly interact with DNA of malignant cells in absence of photosensitizing molecules, ii) fully independent access to imaging and therapeutic modalities, and iii) complete absence of risk of spontaneous activation by natural or artificial light sources other than pulsed femtosecond lasers. Given the unconstrained tunability of the HNPs nonlinear conversion process, this approach can be extended to selectively photo-activate molecules at the surface or in the vicinity of HNPs to further diversify the prospective therapeutic action.[3] Here we show that by tuning the frequency of ultrashort laser pulses from infrared (IR) to visible, SH generation leads respectively to diagnostics (imaging) and therapy (localized phototoxicity). Specifically, we report *in situ* generation of deep ultraviolet (DUV) radiation (270 nm) in human-derived lung cancer cells treated with bismuth ferrite ($BiFeO_3$, BFO) HNPs upon pulsed laser irradiation in the visible spectrum, at 540 nm. We observe and quantify the appearance of double-strand breaks (DSBs) in the DNA and cell apoptosis, in the area of the laser beam. We show that DNA damages are dependent on irradiation-time, laser intensity, and NP concentration. We observe that apoptosis and genotoxic effects are only observed when visible light excitation is employed, being almost completely absent when IR excitation is used for imaging.

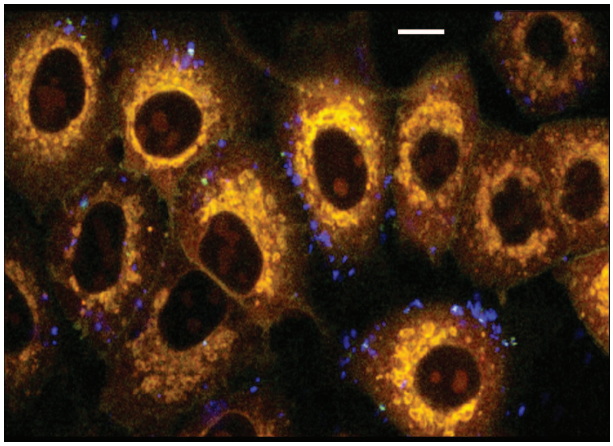

Fig. 1 Multiphoton imaging of a HNPs treated sample. Lung-derived A549 cancer cells exposed for 5 h to 50 μg/mL BFO HNPs. Yellow: two photon excited fluorescence from cell membrane dye FM1-43FX. Blue: SH signal from HNPs. Scale bar:10 μm.

HNPs, a family of NPs specifically conceived for multiphoton imaging, were introduced in 2005 with the aim of complementing fluorescence imaging labels.[1,4,5] Although com-

[a] *Institute of Chemical Sciences and Engineering, EPFL, CH-1015, Lausanne, Switzerland*
[b] *GAP-Biophotonics, Université de Genève, 22 chemin de Pinchat, CH-1211 Genève 4, Switzerland; E-mail: luigi.bonacina@unige.ch*
[c] *FEE Gmbh, Struthstrasse 2, 55743 Idar-Oberstein, Germany*
[d] *SYMME, Université de Savoie, BP 80439, 74944, Annecy Le Vieux Cedex, France*
‡ These authors contributed equally to this work.

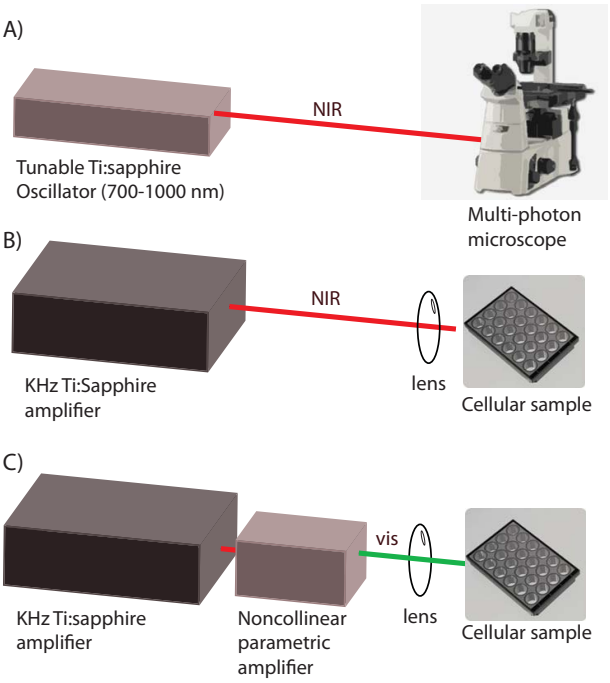

Fig. 2 Different experimental configurations. a) Multiphoton microscope imaging; B) NIR irradiation; C) Visible irradiation.

paratively less bright than quantum dots, HNPs possess a series of advantageous optical properties, including complete absence of bleaching and blinking [1,6], spectrally narrow emission bands, fully coherent response, [7–9] and UV to IR excitation wavelength tunability. [10,11] These unique characteristics have been recently exploited in demanding bio-imaging applications [12] including regenerative medicine research. [13] The possibility of working with long wavelengths presents clear advantages in terms of tissue penetration, as in the IR spectral region, imaging depth is strongly increased by reduced absorption (provided that water absorption bands are avoided) and weak scattering (preventing degradation of spatial and temporal laser profiles). [14]

2 Materials and Experimental Methods

2.1 Multi-photon Imaging

The imaging set-up is based on a Nikon A1R-MP inverted microscope coupled with a Spectra-Physics Mai-Tai DeepSee tunable Ti:Sapphire oscillator (Fig.2a). A Plan APO 40× WI N.A. 1.25 objective was used to focus the excitation laser and to epi-collect the nonlinearly excited signal (SH and membrane dye fluorescence). Four independent non-descanned detectors acquire in parallel the signal spectrally filtered by four tailored pairs of dichroic mirrors and interference filters (SH filter; 395±11 nm, Semrock). Optimal pulse compression at the focal plane was adjusted by maximizing the SH signal of individual HNPs dispersed on a coverslip.

2.2 Visible laser irradiation

For visible irradiation experiments, we employed a two-stage non-collinear optical parametric amplifier (TOPAS White, Light Conversion) set at 540 nm (Fig.2c). The output pulse characteristics are: 30 fs pulse duration, 15 mW average power, 1 KHz repetition rate. For NIR irradiation at 780 nm, the direct output of a Ti:Sapphire amplifier (Coherent Duo Elite CEP) adjusted to yield the same energy, pulse duration, and repetion rate of the visible irradiation experiment was used (Fig.2b). The sample was exposed for 30, 60 and 120 s using a laser spot size (measured by a high resolution beam profiler) of 170 μm or 400 μm diameter obtained by displacing a plano-convex $f = 250$ mm lens.

As for any nonlinear process, the relevant parameter is the pulse peak power at the sample. Due to the very short duration of the pulse employed in this study, the peak power is as high as 2.2 TW/cm^2 or 400 GW/cm^2 for a spot size diameter of 170 μm and 400 μm, respectively. Pulse energy is 15 μJ/pulse in both cases. These values can be compared with those reported by Le Harzic *et al.* [15], who determined cell damage threshold for multi-photon excitation at 517 nm to be above 10 TW/cm^2. Note that due to the ten-fold difference in pulse duration, in our experiment the pulse energy is comparatively less at identical peak-power.

During irradiation, cells were kept at controlled temperature (37^{o}C), CO_2 concentration (5%) and humidity in a portable incubator (Okolab UNO).

2.3 HNPs dispersion and characterization

BFO NPs were provided by the German company FEE under a research agreement at high concentration in ethanol. NPs were diluted 1:50 in 500 mL ethanol and decanted for 10 days. The supernatant was then taken, ethanol evaporated, and NPs re-suspended in distilled water. Successively, NPs were dispersed by ultra-sonic bath for 24 h and quantified by Prussian blue assay. For this assay, 50 μL of BFO solution were diluted in 50 μL HCl 6 M and 100 μL of 5% potassium hexacyanoferrate (Sigma-Aldrich) in PBS were added for 15 min. After incubation, the solution absorbance was measured at 690 nm in a multiwell-plate reader (Synergy HT, BioTek) and compared with the absorbance of a calibration curve with known BFO concentration. BFO NPs were finally diluted at 2 mg/mL in water. DLS and zeta-potential measurements were carried out with a Malvern NanoZ, yielding: zeta potential -52.7 ± 3.5 mV, mean hydrodynamic diameter 165.3 ± 24 nm.

BFO is unanimously considered a very efficient frequency

doubler although presently there is no clear consensus in literature regarding the absolute values of its second-order susceptibility tensor elements. For an order of magnitude, Kumar *et al.* have measured for d_{22} (the largest tensor element) 298 pm/V with 800 nm excitation in a bulk crystal, while Haislmaier *et al.*[16] have reported a d_{22} value of 18.7 pm/V in thin films.[17]

2.4 Cell cultures

Human lung-derived A549 and HTB-182 cancer cell line are available from ATCC (American Tissue Culture Collection). A549 were grown in Dulbecco's Modified Eagle Medium (DMEM) medium containing 4.5 g/L glucose, 10% heat-inactivated fetal calf serum (FCS) and penicillin/streptomycin (PS) (all cell culture reagents were obtained from Invitrogen). HTB-182 were grown in complete Roswell Park Memorial Institute (RPMI) 1640 medium (Invitrogen) supplemented with 10% FCS and PS.

2.5 Cell staining

Cells were grown for 24 h and BFO HNPs at 50 μg/mL were added for further 24 h, then cell layers were fixed in 4% formaldehyde in PBS, permeabilized for 5 min in 0.1% Triton X-100 (Sigma-aldrich) in PBS and exposed to 5 μg/mL of FM1-43FX fluorescent probe (Invitrogen, 1 mg/mL stock solution in DMSO) for 1 min on ice, washed with PBS and maintained in 4% buffered formaldehyde at 4^{o}C until the acquisition of images.

2.6 Determination of cytotoxicity

The cytotoxic effect of BFO HNPs at 100 μg/mL was determined after 5, 24 and 72 h incubation by MTT assay, as previously described.[11] Briefly, after incubation with the BFO or vehicle, MTT solution (3-(4,5-dimethyl-2-thiazoyl)-2,5-diphenyltetrazolium bromide (Sigma-Aldrich) 5 mg/mL in PBS) was added to cells for 2 h. Then, the cell culture supernatants were removed, the cells layers were dissolved in 2-propanol/0.04N HCl and absorbance at 540 nm was measured in a multi-well plate spectrophotometer (Synergy HT, BioTek). Experiments were conducted in triplicate, repeated twice and expressed as cell survival compared to cells exposed to vehicle. Means $\pm$ standard deviations were calculated.

2.7 Dithiothreitol assay

BFO HNPs were diluted at 25 μg/mL or 100 μg/mL in nanopure water containing 250 μM DTT (Sigma-Aldrich) and incubated for 30 min at 37°C, then 90 μL of Ellmann solution (5 mM 5,5'-Dithiobis-(2-nitroben- zoic acid) (DTNB), Sigma-Aldrich) were added and the absorbance was measured at 405 nm in a multiwell-plate reader (Synergy HT). DTT concentration was calculated by comparison with a standard DTT solution. Experiments were conducted in triplicate wells, repeated twice and converted as % of consumed DTT. Means $\pm$ standard deviations were calculated.

2.8 Determination of reactive-oxygen species production

Two different methods were used to determine reactive oxygen species (ROS) production in cells. In the former, ROS were detected by measuring the oxidation of DHE to ethidium. Cells were grown for 24 h and BFO at 25 μg/mL or 100 μg/mL were added for further 24 h. Then, cell layers were washed with PBS and 100 μM DHE (Sigma-Aldrich) in RPMI 1640 were added for 15 min at 37°C. Cells layers were further washed and lysed with 0.1% Triton X-100 (Sigma-Aldrich) in PBS. Ethidium production was determined in a fluorescent multiwell-plate reader (Synergy HT) at $\lambda_{ex}/\lambda_{em}$ = 485/580 nm.

The second ROS measurement method involved the use of DCFH-DA.[18] DCFH-DA is trapped inside cells as a sensitive cytosolic marker of oxidative stress, since its oxidation leads to the formation of the fluorescent dichlorofluorescein (DCF). Cells were grown and treated with BFO as previously described, then cells layers were washed with PBS and exposed to 20 μM DCFH-DA in Hank's buffer solution (HBSS) (both from Invitrogen) for 40 min at 37^{o}C. After incubation, the cell layers were further washed and fluorescence of DCF was measured at $\lambda_{ex}/\lambda_{em}$ = 485/527 nm. Experiments were conducted in triplicate, repeated twice and expressed as fold-increase compared to cells exposed to vehicle. Means $\pm$ standard deviations were calculated.

2.9 Immunohistochemistry

Fixed cell layers were washed twice with PBS, permeabilized with cold methanol (-20°C) for 5 min, washed with PBS and incubated 10 min at RT in 3% H_2O_2 in methanol. Then, cells were washed and incubated for 1.5 h at RT with anti-phospho-histone H2AX (Ser139) or anti-cleaved PARP antibodies (both from Cell Signaling) diluted 1:250 in Dako REALTM Antibody Diluent (Dako). After incubation, cell layers were washed twice with PBS and incubated with undiluted anti-rabbit HRP-conjugate antibody (EnVision+ Sytem, Dako) for 30 min at RT. Cells were further washed and HRP activity was revealed using the DAB+ CHROMOGEN system from Dako, according to the supplier instructions. Finally, cells were counterstained with hematoxylin and images were taken using a microscope (DM IL LED from Leica) equipped with a digital camera (ICC50HD, Leica). Three pictures per treatment were taken and positive cells in a surface of 0.3 mm^2 around the laser-spot were counted using the ImageJ

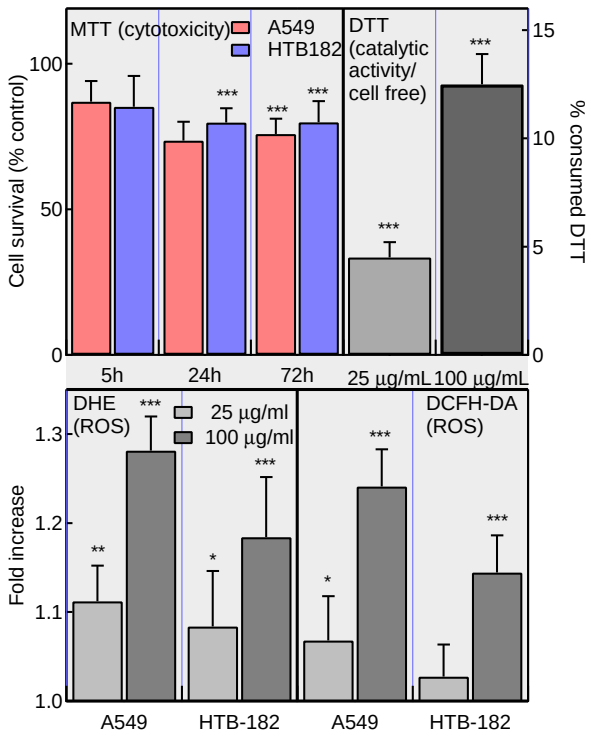

Fig. 3 Cytotoxic and oxidative effects of BFO HNPs.
MTT. Cell survival by MTT for different exposure times of lung-derived A549 (red) and HTB-182 (blue) cancer cell lines exposed to 100 μg/mL BFO.
DTT. Effect of BFO at 25 and 100 μg/mL on DTT content in an abiotic environment after 1 h of incubation.
DHE DCFH-DA. ROS production after 24 h exposure to 25 or 100 μg/mL HNPs by DHE and DCFH-DA assays. Results statistically compared to untreated cells.
†: $p > 0.05$; $*p < 0.05$; ** $p < 0.01$; *** $p < 0.001$.

software. Experiments were conducted in triplicate wells, repeated twice and expressed as % of positive cells per picture.

2.10 Statistical analysis

Data were compared using a homoscedastic, two-tailed distributed Student's t-test. Details about comparisons are specified in the caption of each figure. Significance is expressed as: †: $p > 0.05$; * $p < 0.05$; ** $p < 0.01$; *** $p < 0.001$.

3 Results

As an example of HNPs based imaging, figure 1 displays lung-derived A549 cancer cells stained with FM1-43FX cell membrane dye exposed for 5 h to BFO HNPs at 50 μg/mL. The image was acquired upon near IR excitation at 790 nm, the two-photon excited fluorescence from the dye is shown in yellow, while the intense blue spots correspond to SH radiation emitted by HNPs. The latter have the tendency to remain attached to cell membranes without being internalized due to their relatively large size. As for other nanobiotechnological approaches, selective binding of NPs to specific cell membrane receptors would rely on the presence of targeting molecules at their surface,[12] a strategy that was not implemented in this exploratory study.

3.1 BFO Cytotoxicity and ROS production

Given the novelty of the nanomaterial employed in this work, prior to the assessment of photo-therapeutic modality, BFO HNPs were characterized and screened for biocompatibility in terms of cytotoxicity and oxidative effect. As reported in figure 3 MTT, the cytotoxic effect of 100 μg/mL BFO HNPs was assessed after 5, 24 and 72 h exposure on two lung-derived cell lines (A549, HTB-182). BFO cytotoxicity was found acceptable in both samples as HNPs did not cause any detectable effect on cell survival after 5 h exposure, and after 24 h and 72 h cell viability remains remarkably high (>75%), comparable to that observed with HNPs composed of other nanomaterials previously screened.[11]

In the present work, it is of paramount importance to precisely quantify ROS production by NPs to identify their possible role in the therapeutic protocol described below. The catalytic activity of BFO HNPs was first measured in a cell free environment by dithiothreitol (DTT) assay.[19] The histogram of figure 3 DTT indicates that BFO HNPs do indeed show a dose-dependent consumption of DTT after 1 h incubation, suggesting that they can exert catalytic production of superoxide. On the ground of this finding, we determined the ROS production by BFO HNPs in cell cultures using two fluorescence assays: dihydroethidium (DHE) and carboxydichlorodihydrofluorescein diacetate (DCFH-DA).[18,20] We could detect a dose-dependent increase of ROS, more pronounced in A549 cells than in HTB-182 (figure 3 DHE and DCFH-DA). We point out that ROS production remains however low compared to that induced by other metal-based NPs:[11,18,20,21] for a quick comparison, human fibroblast exposed for 2 and 5 h to 25 μg/mL of Ag nanoparticles yields a three-fold increase in the DHE output, similar to the positive control (H_2O_2) tested by AshaRani *et al.*.[20] Overall, the result of this thorough screening indicates a good biocompatibility of this nanomaterial, tested for the very first time for biological applications, and sets the ground for the light-triggered HNPs-cells interaction described in the following.

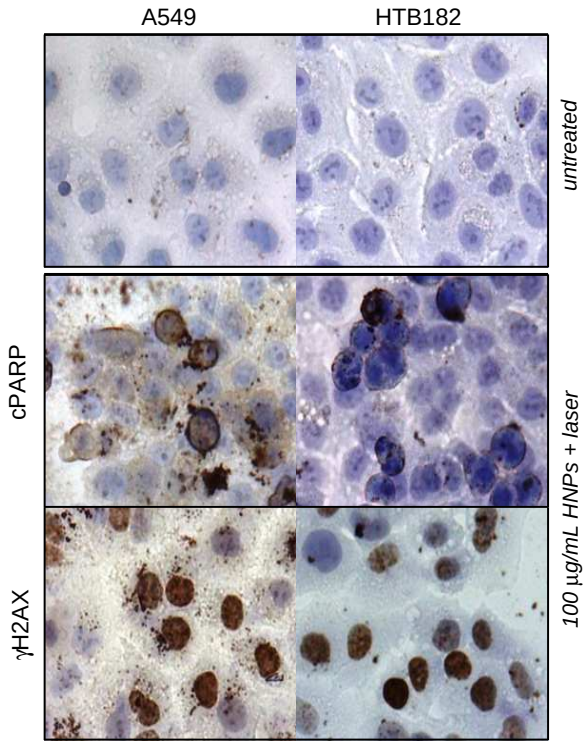

Fig. 4 Immunohistochemistry. Human lung-derived A549 and HTB-182 cancer cell lines untreated (first row) or exposed to 100 μg/mL BFO HNPs (**2** and **3**), incubated 24 h, and irradiated at 540 nm for 120 s. The expression of cPARP (fourth row) and γH2AX (third row) observed by IHC after further 24 h or 30 min of incubation, respectively. Positive cells are in brown, nuclei in blue, and HNPs aggregates appear as small brown spots.

3.2 Laser irradiation experiments

DNA absorption is particularly efficient in the deep UV (DUV, $<$300 nm), as all DNA bases possess absorption bands peaking around 260 nm with negligible intensity from 310 nm on. Irradiation of cell cultures at this wavelength results into DSBs and evokes a complex network of molecular responses, eventually resulting in DNA repair and/or cell apoptosis.[22–24] In our work, these two different biological phenomena were monitored performing two *ad hoc* bioassays: γH2AX and cPARP, respectively.

Histone variant H2AX is a key component of the early stage response to DNA damages, as upon UV exposure it is phosphorylated at its carboxyl terminus to form γH2AX at the DSBs sites.[22,23,25,26] After the first appearance of UV-induced DNA-damages, cells first activate DNA-repair mechanisms and then apoptosis occurs to eliminate potentially hazardous cells. UV-dependent apoptosis is caused by the activation of caspase-3 and subsequently cleavage of the poly (ADP-ribose) polymerase (PARP), resulting in a cleaved-form (cPARP) with a mass of 89 kDA.[26–28]

For the irradiation experiment, cells were plated in 35 mm Petri dishes with glass bottom for 48 h, then medium was replaced and cells were incubated for 24 h with BFO HNPs (25 or 100 μg/mL, 2 mg/mL stock solution in water) or a negative control containing the vehicle (distilled water). The sample was exposed for 30, 60, or 120 s to ultrashort (30 fs) pulses of visible light with a laser spot size of 170 μm diameter. During irradiation, cells were kept in stable conditions in a portable incubator. After light treatment, cells were incubated for 30 min (γH2AX assay) or 24 h (cPARP assay)[25,29,30] and then fixed with 3% formaldehyde in PBS. Frequency doubling of femtosecond pulses of visible light (540 nm) by HNPs attached to cell membranes generates DUV photons in the close vicinity of cell nuclei, optimally placed for direct photo-interaction (see figure 1). The biological effects of such laser irradiation is reported in the immunohistochemistry (IHC) images of figure 4. The two columns are associated to the two human malignant cell lines already tested for cytotoxicity, A549 and HTB-182. The control samples (first row) show no expression for both reporters, confirming that they are not present under physiological conditions, while the clear effect (positive cells in brown) visible in rows two and three for treated (exposed to HNPs and laser) cells indicates that a strong interaction upon irradiation takes places, showing the DNA-repairing enzyme γH2AX expression well localized within the nuclei and the cPARP reporter of cell apoptosis in the cytoplasm of the damaged cells.

The spatial localization of the IHC expression of the two reporters for DNA repair and cell apoptosis is given in figure 5. The laser focal spot (empty white square) is superimposed to a spatially resolved pattern of $80 \times 130 \mu$m rectangles indicating

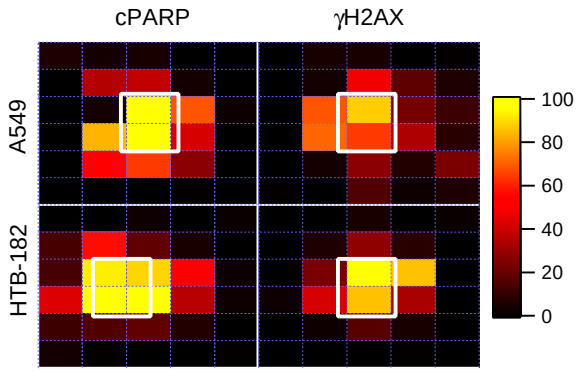

Fig. 5 Spatial localization of the expression of cPARP and γH2AX reporters. Analysis of one representative IHC image (480 x 650 μm) for the treatments in figure 4. For each rectangular (80 $\times$ 130 μm) data region the % ratio of cells positive for the expression of cPARP (column 1) and γH2AX (column 2) is expressed in false colors according to the colorbar. Black empty square: laser spot region (170 $\times$ 170 μm^2).

in false colors the % of positive cells to cPARP and γH2AX for both cell lines. One can appreciate how the biological effect of visible irradiation strongly co-localizes with the laser spot (>80 % positive cells) and rapidly decreases outside the focal region to negligible values.

The quantitative assessment of the effects of *in situ* DUV generation is reported in the comprehensive figure 6. In the histograms, the number of IHC-positive cells is expressed as % ratio of total cells in the area of the laser-spot. Firstly, one can observe that BFO HNPs at 25 and 100 μg/mL without laser irradiation do not cause any significant increase of cPARP and γH2AX expression, ensuring that oxidative and cytotoxic effects of BFO alone do not interfere with irradiation assays.

Upon laser-exposure, the ratio of cells positive for cPARP and γH2AX clearly increases in an exposure time-dependent manner. Cells treated with 25 μg/mL show a reduced expression of cPARP as compared to those exposed to 100 μg/mL, which remains anyway always significantly greater than that measured with vehicle. This decrease in expression is more pronounced for HTB-182 cells. The number of positive cells for γH2AX expression decrease in the two cell lines accordingly.

In A549 the expression of the two proteins is comparable, whereas HTB-182 express systematically more γH2AX. Such a stronger DNA-repair related enzymatic activity seems correlated with higher cell viability: the maximal expression of cPARP (apoptosis) is around 60% while in A549 it reaches almost 100%.

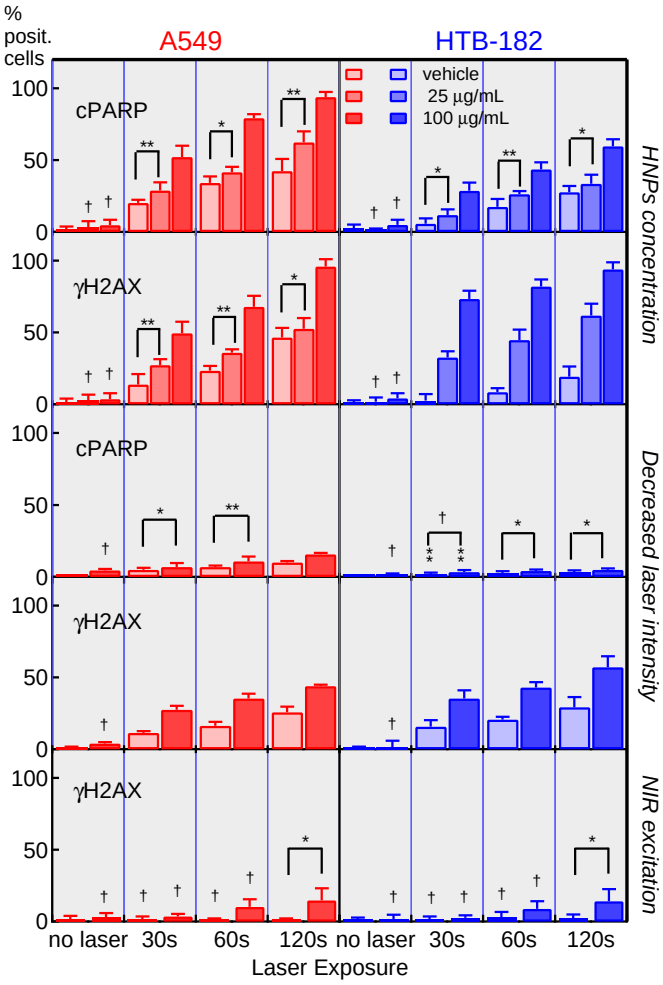

Fig. 6 Statistical analysis. All results are expressed as % ratio of positive cells. Samples exposed to nanoparticles were compared to samples exposed to vehicle using the Student t-test: All comparisons are significant ($p < 0.001$) if not otherwise specified.
†: $p > 0.05$; $*p < 0.05$; ** $p < 0.01$.
HNPs concentration. Expression of cPARP (first row) and γH2AX (second row) for A549 (left, red) and HTB-182 (right, blue) cancer cell lines exposed to vehicle, 25, or 100 μg/mL BFO HNPs, incubated 24 h and irradiated for 30, 60, or 120 s at 540 nm following the high intensity protocol.
Decreased laser intensity. Expression of cPARP (third row) or γH2AX A549 (fourth row) for the same cell lines exposed to vehicle or 100 μg/mL BFO HNPs , incubated 24 h and irradiated for 30, 60 or 120 s at 540 nm following the five-fold lower intensity protocol.
NIR excitation. Expression of γH2AX for cells exposed to vehicle or 100 μg/mL BFO HNPs, incubated for 24 h and irradiated for 30, 60, or 120s at 780 nm at maximal intensity.

To complete the characterization of the HNPs+visible irradiation synergistic effects on cells viability, we further investigated laser intensity and HNP concentration dependence. A549 and HTB-182 cells were exposed to 100 μg/mL HNPs or vehicle and irradiated with the same laser average power focused onto a larger surface (400 μm diameter), corresponding to a neat fivefold intensity decrease with respect to the previous irradiation protocol. As reported in the third and fourth rows of figure 6, a substantial decrease in the expression of both cPARP and γH2AX was detected in both cancer cell lines. However, the difference between cells treated with BFO and with vehicle remained always significant, except for the expression of cPARP on HTB-182 cells after 30 s exposure, suggesting that BFO generate DUV at lower irradiation intensity as well. The greatest difference between cells exposed to BFO and to vehicle was always observed for the longest exposure and the decrease on cPARP expression was greater compared to the expression of γH2AX. The dramatic reduction in cPARP is consistent with the square intensity dependence of the second harmonic process at the basis of the NPs-cells interaction.

The major decrease in cells viability observed upon irradiation of HNPs-treated samples, together with the high spatial localization of the biological effects (figure 5, makes HNPs-based approaches amenable for developing therapeutic (photo-dynamic) protocols. To assess the wavelength-dependent multi-modality of the method, immunochemistry was performed also for imaging only modality. Cells exposed to 100 μg/mL were irradiated at 780 nm (SHG at 390 nm, outside the DNA bases absorption band) with the same pulse intensity and laser repetition rate as for the data presented in the first two rows of figure 6. Expression of γH2AX and cPARP was detected according to the protocol previously described. Compared to 540 nm laser excitation, the percentage of positive cells for γH2AX is significantly lower at this longer wavelength, and no expression of cPARP was observed under all exposure conditions. As reported in previous works, using the HNPs approach, imaging is not limited to near infrared wavelengths but it can be performed even above 1.5 μm, with clear advantages in terms of imaging penetration depth (thanks to decreased scattering and absorption) [1,10] and decreased phototoxicity.

4 Discussion

The results and control experiments presented altogether confirm that UV generation and related cytotoxic and genotoxic effects can be unambiguously ascribed to BFO HNPs nonlinearly excited by ultrashort *visible* light pulses. Major effects on cell viability (up to 100% apoptosis) are observed in the irradiated areas. The difference on γH2AX expression between cells irradiated with lower laser intensity or exposed to lower particle concentration suggests that the synergistic effect between laser and HNPs is dominated by direct DNA photo-damages, but they might also implies other subsidiary mechanisms, suggested in the literature, such as a thermal effects and cell membranes disruption. [31–33] The apoptotic cell fraction in samples exposed to 540 nm laser but not treated with HNPs (cells exposed to vehicle in the histograms in the first and second row of figure 6) can be ascribed to direct two-photon absorption by DNA, as previously observed in other works. [34,35]

Non HNP-specific interaction can be easily counteracted thanks to the fact that the cellular effects exerted by BFO HNPs are limited to the area of the laser spot, as highlighted in figure 5. If IR imaging is preliminary performed to precisely define the zone needing irradiation, treatment conserves its high specificity. It should be noted that treatment localization is expected to be greater in the proposed HNP-based approach, which is primarily based on direct UV absorption by DNA, than in photo-dynamic treatments involving direct UV irradiation or upconverting and plasmonic NPs combined with photo-sensitizing drugs. In these latter cases, NPs-cell interaction is essentially mediated by ROS, which are known to diffuse through tissues. [36,37]

It is worth pointing out that all optical methods listed are limited to surface neoplasms that can be accessed either directly either endoscopically, as optical penetration depth in tissues (strongly depending on the wavelength) remains limited at best to a few millimetres. On the positive side, the proposed approach shares the advantages of nonlinear techniques, enabling to maximize penetration. Moreover, and notably, the activation of the process here is intrinsically limited to femtosecond-pulse excitation and cannot be obtained by any other artificial or natural light source, differently also from the approaches based on sequential up-conversion of light frequency. This purely physical constrain greatly decreases the risk of unspecific treatment activation for surface lesions. Beyond medical approaches, we believe that the proposed approach can be used for biological applications to photo-trigger in vitro or tissues with high degree of spatial selectivity, for example grafting on HNPs some photo-cleavable molecules or taking advantage of DUV generation for protein cross-linking.

5 Conclusions

In conclusion, we have presented and demonstrated on human-derived cancer cell lines an original nanobiotechnological approach based on the nonlinear optical properties of HNPs. The proposed method enables wavelength-selected imaging and direct DUV generation and photo-interaction with nuclear DNA. The biocompatibility of BFO, a nanomaterial firstly applied for biological applications to the best of our knowledge, screened for cytotoxicity and generation of oxida-

tive stress, was found comparable to those of other HNPs or metal-based nanoparticles currently used in biomedical studies.[11,18,20,21] It should be noted that all HNPs, possessing high nonlinear efficiency,[11] can exert the effects described in this study, which are therefore not unique to BFO.

DSBs DNA damages and induction of apoptosis are typical targets of photodynamic therapies, which normally involved the use of direct UV radiation (with poorer tissue penetration and lack of specificity) and/or chemical photosensitizers.[38,39] To date, NPs-based strategies imply using of organic sensitizers (with some notable exceptions.[40]) and are mediated by ROS generation.[21,37,41,42] As for classical phototherapy, these approaches can generate major side effects due to the presence of toxic compounds and ROS which can diffuse to nearby tissues generating oxidative stress.[43,44] The approach proposed, based on nonlinear optical response by HNPs and direct photo-interaction with nuclear DNA, might avoid side effects due to organic ligands and diffusion of toxic compounds, increasing selectivity and treatment localization. Finally, and very notably, the proposed strategy allows to totally decouple diagnostic modality (IR imaging) from the therapeutic photo-dynamic action (visible irradiation), by simply tuning the excitation laser wavelength.

6 Acknowledgements

This research has been conducted in the framework of European FP7 Research Project NAMDIATREAM (NMP4-LA-2010-246479, http://www.namdiatream.eu). The authors thank MER Dr Christine Wandrey for granting access to analytical equipment and S. Afonina and J. Gâteau for assistance with femtosecond laser equipment.

References

1 L. Bonacina, Y. Mugnier, F. Courvoisier, R. Le Dantec, J. Extermann, Y. Lambert, V. Boutou, C. Galez and J. P. Wolf, *Applied Physics B-Lasers and Optics*, 2007, **87**, 399–403.

2 W. P. Dempsey, S. E. Fraser and P. Pantazis, *Bioessays*, 2012, **34**, 351–60.

3 H. Zhao, E. S. Sterner, E. B. Coughlin and P. Theato, *Macromolecules*, 2012, **45**, 1723–1736.

4 Y. Nakayama, P. J. Pauzauskie, A. Radenovic, R. M. Onorato, R. J. Saykally, J. Liphardt and P. Yang, *Nature*, 2007, **447**, 1098–101.

5 P. Pantazis, J. Maloney, D. Wu and S. E. Fraser, *Proc Natl Acad Sci U S A*, 2010, **107**, 14535–40.

6 L. Le Xuan, C. Zhou, A. Slablab, D. Chauvat, C. Tard, S. Perruchas, T. Gacoin, P. Villeval and J. F. Roch, *Small*, 2008, **4**, 1332–1336.

7 R. Baumner, L. Bonacina, J. Enderlein, J. Extermann, T. Fricke-Begemann, G. Marowsky and J. P. Wolf, *Optics Express*, 2010, **18**, 23218–23225.

8 C. L. Hsieh, R. Grange, Y. Pu and D. Psaltis, *Optics Express*, 2010, **18**, 3456–3457.

9 C. L. Hsieh, Y. Pu, R. Grange, G. Laporte and D. Psaltis, *Optics Express*, 2010, **18**, 20723–20731.

10 J. Extermann, L. Bonacina, E. Cuna, C. Kasparian, Y. Mugnier, T. Feurer and J. P. Wolf, *Optics Express*, 2009, **17**, 15342–15349.

11 D. Staedler, T. Magouroux, R. Hadji, C. Joulaud, J. Extermann, S. Schwungi, S. Passemard, C. Kasparian, G. Clarke, M. Gerrmann, R. Le Dantec, Y. Mugnier, D. Rytz, D. Ciepielewski, C. Galez, S. Gerber-Lemaire, L. Juillerat-Jeanneret, L. Bonacina and J. P. Wolf, *ACS Nano*, 2012, **6**, 2542–2549.

12 J. Culic-Viskota, W. P. Dempsey, S. E. Fraser and P. Pantazis, *Nature Protocols*, 2012, **7**, 1618–1633.

13 T. Magouroux, J. Extermann, P. Hoffmann, Y. Mugnier, R. Le Dantec, M. E. Jaconi, C. Kasparian, D. Ciepielewski, L. Bonacina and J. P. Wolf, *Small*, 2012, **8**, 2752–2756.

14 W. R. Zipfel, R. M. Williams and W. W. Webb, *Nature Biotechnology*, 2003, **21**, 1368–1376.

15 R. Le Harzic, I. Riemann, K. Konig, C. Wullner and C. Donitzky, *Journal of Applied Physics*, 2007, **102**,2077.

16 R. C. Haislmaier, N. J. Podraza, S. Denev, A. Melville, D. G. Schlom and V. Gopalan, *Applied Physics Letters*, 2013, **103**, 031906–031906–4.

17 A. Kumar, R. C. Rai, N. J. Podraza, S. Denev, M. Ramirez, Y.-H. Chu, L. W. Martin, J. Ihlefeld, T. Heeg and J. Schubert, *Applied Physics Letters*, 2008, **92**, 121915–121915–3.

18 R. Frick, B. Muller-Edenborn, A. Schlicker, B. Rothen-Rutishauser, D. O. Raemy, D. Gunther, B. Hattendorf, W. Stark and B. Beck-Schimmer, *Toxicol Lett*, 2011, **205**, 163–72.

19 A. K. Cho, C. Sioutas, A. H. Miguel, Y. Kumagai, D. A. Schmitz, M. Singh, A. Eiguren-Fernandez and J. R. Froines, *Environ Res*, 2005, **99**, 40–7.

20 P. V. AshaRani, G. Low Kah Mun, M. P. Hande and S. Valiyaveettil, *ACS Nano*, 2009, **3**, 279–90.

21 A. Barzilai and K. Yamamoto, *DNA Repair (Amst)*, 2004, **3**, 1109–15.

22 S. Hanasoge and M. Ljungman, *Carcinogenesis*, 2007, **28**, 2298–304.

23 J. Yuan, R. Adamski and J. Chen, *FEBS Lett*, 2010, **584**, 3717–24.

24 L. Stergiou, R. Eberhard, K. Doukoumetzidis and M. O. Hengartner, *Cell Death Differ*, 2011, **18**, 897–906.

25 C. Lu, F. Zhu, Y. Y. Cho, F. Tang, T. Zykova, W. Y. Ma, A. M. Bode and Z. Dong, *Mol Cell*, 2006, **23**, 121–32.

26 M. F. Shih and J. Y. Cherng, *Molecules*, 2012, **17**, 9116–9128.

27 R. Takasawa, H. Nakamura, T. Mori and S. Tanuma, *Apoptosis*, 2005, **10**, 1121–30.

28 C. Tuchinda, H. W. Lim, F. M. Strickland, E. A. Guzman and H. K. Wong, *Photodermatol Photoimmunol Photomed*, 2007, **23**, 2–9.

29 E. R. Lee, J. H. Kim, Y. J. Kang and S. G. Cho, *Biol Pharm Bull*, 2007, **30**, 32–7.

30 S. Narayanapillai, C. Agarwal, C. Tilley and R. Agarwal, *Photochem Photobiol*, 2012, **88**, 1135–40.

31 Y. Aragane, D. Kulms, D. Metze, G. Wilkes, B. Poppelmann, T. A. Luger and T. Schwarz, *J Cell Biol*, 1998, **140**, 171–82.

32 X. Huang, P. K. Jain, I. H. El-Sayed and M. A. El-Sayed, *Lasers Med Sci*, 2008, **23**, 217–28.

33 J. Li, D. Guo, X. Wang, H. Wang, H. Jiang and B. Chen, *Nanoscale Res Lett*, 2010, **5**, 1063–71.

34 K. Konig, P. T. C. So, W. W. Mantulin and E. Gratton, *Optics Letters*, 1997, **22**, 135–136.

35 U. K. Tirlapur, K. Konig, C. Peuckert, R. Krieg and K. J. Halbhuber, *Experimental Cell Research*, 2001, **263**, 88–97.

36 N. M. Idris, M. K. Gnanasammandhan, J. Zhang, P. C. Ho, R. Mahendran and Y. Zhang, *Nature Medicine*, 2012, **18**, 1580–U190.

37 A. Zhou, Y. Wei, B. Wu, Q. Chen and D. Xing, *Mol Pharm*, 2012, **9**, 1580–9.

38 T. Offer, B. N. Ames, S. W. Bailey, E. A. Sabens, M. Nozawa and J. E. Ayling, *Faseb J*, 2007, **21**, 2101–7.

39 A. R. Soares, M. G. Neves, A. C. Tome, M. C. Iglesias-de la Cruz, A. Zamarron, E. Carrasco, S. Gonzalez, J. A. Cavaleiro, T. Torres, D. M. Guldi and A. Juarranz, *Chem Res Toxicol*, 2012, **25**, 940–51.

40 L. Minai, D. Yeheskely-Hayon, L. Golan, G. Bisker, E. J. Dann and D. Yelin, *Small*, 2012, **8**, 1732–1739.

41 B. Ungun, R. K. Prud'homme, S. J. Budijon, J. Shan, S. F. Lim, Y. Ju and R. Austin, *Opt Express*, 2009, **17**, 80–6.

42 C. Wang, H. Tao, L. Cheng and Z. Liu, *Biomaterials*, 2011, **32**, 6145–54.

43 K. Jomova, S. Baros and M. Valko, *Transition Metal Chemistry*, 2012, **37**, 127–134.

44 N. Scola, S. Terras, D. Georgas, N. Othlinghaus, R. Matip, I. Pantelaki, K. Mollenhoff, M. Stucker, P. Altmeyer, A. Kreuter and T. Gambichler, *Br J Dermatol*, 2012, **167**, 1366–73.